# The creation of three-dimensional finite element models for simulating head impact biomechanics

T J Horgan and M D Gilchrist*

*Department of Mechanical Engineering, University College Dublin, Ireland*

**Abstract**: A new 3 dimensional finite element representation of the human head complex has been constructed for simulating the transient occurrences of simple pedestrian accidents. This paper describes the development, features and validation of that model. When constructing the model, emphasis was placed on element quality and ease of mesh generation. As such, a number of variations of the model were created. The model was validated against a series of cadaveric impact tests. A parametric study (a High/Low study) was performed to investigate the effect of the bulk and shear modulus of the brain and cerebrospinal fluid (CSF). The influence of different mesh densities on the models and the use of different element formulations for the skull were also investigated. It was found that the short-term shear modulus of the neural tissue had the predominant effect on intracranial frontal pressure, and on the predicted Von-Mises response. The bulk modulus of the fluid had a significant effect on the contre-coup pressure when the CSF was modelled using a coupled node definition. Differences of intracranial pressure were reported that show the sensitivity of the method by which the skull is modelled. By simulating an identical impact scenario with a range of different finite element models it has been possible to investigate the influence of model topologies. We can conclude that careful modelling of the CSF (depth/volume) and skull thickness (including cortical/trabecular ratio) is necessary if the correct intracranial pressure distribution is to be predicted, and so further forms of validation are required to improve the finite element models' injury prediction capabilities.

## NOTATION

| | |
|---|---|
| $\beta$ | Decay factor |
| $\lambda_X, \lambda_Y, \lambda_Z$ | $X$, $Y$ and $Z$ dimension length scale factors |
| $C_{10}, C_{01}$ | Temperature dependent coefficients |
| $G_0$ | Short term shear modulus |
| $G_\infty$ | Long term shear modulus |
| $t$ | Time |

## INTRODUCTION

The head is one of the most frequently injured body regions and neurotrauma constitutes one of the major causes of death in accidents. Despite increased use of seat belts and helmets, brain injury disables or fatally injures someone in the United States every two and a half minutes. The estimated annual costs for hospitalisation and rehabilitation of head injured patients is estimated at 25 billion dollars [1]. The engineering aim of injury biomechanics research is to develop ways of simulating the trauma that can occur from impact by applying the principles of mechanics. This can only be achieved by first understanding the mechanisms of impact injury and the biomechanical response of the head-brain system to a variety of loading conditions. Traumatic brain injury mechanisms are described in terms of the mechanical and physiological changes that result in anatomical and functional damage. Due to its complex nature, functional damage is difficult to quantify and it is for this reason that a variety of alternative mechanisms have been proposed for explaining the development of brain injury. All theories, however, agree that injury is related to acceleration of the head regardless of whether the impact is applied directly or indirectly.

The brain is loosely coupled to the skull with the effect that its motion will lag that of the skull, resulting in 'bruising' of the brain as it impacts against the interior surface of the skull. Stretching of the tethering blood vessels, which arises as a result of this lag in motion, can

*Corresponding Author*:*
Dr Michael D Gilchrist, FInstP, FIMechE, FIEI, Department of Mechanical Engineering, University College Dublin, Belfield, Dublin 4, Ireland
Tel +353 1 7161890 Fax +353 1 2830534
Email: michael.gilchrist@ucd.ie

cause them to strain excessively, rupture, fail and bleed. The brain tissue itself may be damaged by normal and shear forces that develop during translational and rotational accelerations or decelerations.

The constitutive properties of both the skull and brain characterise the system response to mechanical loads and must be known if the physical response of the skull–brain system is to be predicted accurately. This has posed significant difficulties for researchers in recent decades following the development of adequate computational resources, since the properties of living human tissue deviate from those of cadavers and primates and harmless non-invasive procedures for establishing such properties *in vivo* have not been established.

Experimental studies have been carried out using animals, cadavers, dummies and other physical models. The general method is to measure forces, accelerations and/or displacements and relate these physical parameters to tolerances, severity, types and criteria of traumatic injury. The findings of such experimental studies may also be used to validate mathematical models, where the impact conditions are pre-defined and a solution attempts to predict future injuries.

Many tests have been conducted on cadavers to provide information concerning the various processes involved in impact of the head. The primary advantage of cadaveric studies is that they have the same geometry and mass distribution as a living human, although pathophysiological differences, and therefore information pertaining to the mechanisms of damage, cannot be studied with such tests. Cadaver skulls have been studied where geometry has been of importance [2], although it is unclear how bone properties would deteriorate due to drying or embalming.

Perhaps the most widely recognised cadaveric study was performed by Nahum et al. [3] who investigated two series of cadaver head impact experiments, the first consisting of single impact experiments and the other focusing on repeated impacts of different energy levels to a single specimen. The specimens were prepared in order that in vivo fluid pressures within the cerebrospinal fluid (CSF) space and cerebral blood vessels could be measured. The seated, stationary cadaver subjects were impacted by a rigid mass travelling at a constant velocity. The blows were delivered to the frontal bone in the mid-sagittal plane in an anterior–posterior direction. Both the input force time histories and the intracranial pressure time histories were recorded.

Analytical modelling, which has largely been superseded by finite element methods within the past two decades, represents the head/brain either as a fluid filled shell or a combined mass-spring-damper system. Lumped parameter models merely define the gross rheological and/or structural response. Continuum models are more desirable for defining head injury since they can predict local phenomena such as displacements, stresses, strain rates and wave propagation.

Misra and Chakravarty [4] performed an analysis that considered the eccentricity of the cranium by modelling the head as a prolate spheroidal shell (i.e., ellipsoid) filled with linear viscoelastic material representing the brain. The effect of an angular acceleration pulse was studied. The numerical investigation was based on a finite difference approach. It was calculated that an angular acceleration of magnitude greater than $20 \times 10^3$ rad/s$^2$ should cause human brain injury. The model however, considered the skull brain system to be floating whereas in reality the motion of the head is influenced by the neck and its muscles and ligaments which limits the applicability of this model.

The diverse analytical approaches have largely used closed form solutions based on idealised geometry and boundary conditions. With the development of finite element methods four decades ago, biomechanics research took on a new direction. The finite element method is a computational technique that is used to obtain approximate solutions to the sets of partial differential equations that predict the response of physical systems that are subjected to external influences. Finite element modelling can be used to elucidate and predict the mechanical and physical response of a brain to impact loadings. Accurate predictions and optimum results from such a technique can only be obtained by first establishing a geometrically and constitutively accurate model of the skull brain system. In principle, finite element models can be used for exploring complex geometries, non-linearities and variable impacts. Within recent years, this computational technique has become more powerful and less expensive to the extent that it is commonly recognised as the best tool for analysing the response of the head to complicated loading conditions.

## PHYSIOLOGICAL CONSIDERATIONS

The skull has often been modelled as a sphere, but in reality it is closer to an ellipsoid that is narrower towards the front of the head. It has been suggested by many [5, 6, 7] and confirmed analytically [4] and computationally [8] that this eccentricity will influence the response of the head to an impact. The frontal bone provides greater resistance to stress due to its curvature. If the skull is represented by a discrete distribution of sprung masses, the stiffness of the skull would be different for each impact scenario because the structural response is dependent on all of the springs involved. In addition, the radius of curvature of the skull is different throughout: in some areas it is much more rounded while in others it is much flatter.

The cerebrospinal fluid acts as an important energy damping mechanism during impact of the skull brain system. Higher contrecoup injuries have been witnessed when high accelerations before impact are involved, such as develop in a fall where the head is rapidly decelerated upon contacting the stationary ground. This has been attributed to the theory that, during the fall, the cerebrospinal fluid moves towards the impact site leaving

the contrecoup site relatively deficient. This has been confirmed experimentally [9]. Cerebrospinal fluid has been seen to reduce the magnitude of the shear strains near the falx, the partition between the cerebral hemispheres, when the head is subject to rotational impact about the horizontal plane. Also, the theory of cavitation largely depends on the presence of cerebrospinal fluid near the brain. All this implies that careful modelling of the cerebrospinal fluid is essential when analysing the response of the brain to an impact. The subarachnoid space, in which the cerebrospinal fluid is contained, is non existent over the surfaces of the gyri, is relatively small where the arachnoid bridges over small sulci and is much larger in certain locations where it bridges over large surface irregularities. Such regions, containing a considerable volume of cerebrospinal fluid are called subarachnoid cisterns. However the current analysis has treated the cerebrospinal fluid as a layer of uniform depth, as has been done previously [8, 10–12].

Boundary conditions, such as the foramen magnum (the opening at the base of the skull), must also be considered carefully in any representative model. The presence of the foramen magnum allows the intracranial pressure to change during and subsequent to an impact. Representing the foramen magnum by a force free opening in combination with a no-slip interface [13] is likely to impose too strong a constraint on the movement of the brain through the opening for the spinal cord. Sauren & Claessens [14] suggested that using a slip condition at the skull-brain interface, together with a small opening around the spinal cord to represent the foramen, might provide a more realistic numerical solution. The kinematic neck boundary condition must also be modelled to allow the head respond realistically to impact. The most reasonable boundary condition probably depends on the impact condition (i.e., the distance from the head neck junction, regardless of whether the accelerations are translational or rotational) and these would allow some simplifying assumptions to be made in any model.

## MODEL CONSTRUCTION

The geometry of a male and a female human cadaver has been determined by Computed Tomography (CT), Magnetic Resonance Tomography (MRT) and sliced colour photographs. The geometric data are available through the Visible Human Database (National Institute of Health, USA [15]) with 0.3 mm incrementation in the coronal plane. The current model was created using this CT data. Such digitised data is made up of voxels, which can be considered to be three-dimensional pixels. The scans are stored in stacks therefore making up a stepped volume sampled recording. Interpolation and thresholding schemes are then implemented to identify voxels representing bone, for example, and then interpolate through the voxel generating smooth triangle surfaces closer to the shape of the actual scanned head. The CT data was used to create a polygonal model of the visible male skull using vtk-software [16]. The resulting polygonal model was decimated and smoothed in order to make the model more portable [See Fig. 1]. This then was converted into IGES format and imported into the commercially available software MSC/Patran [17].

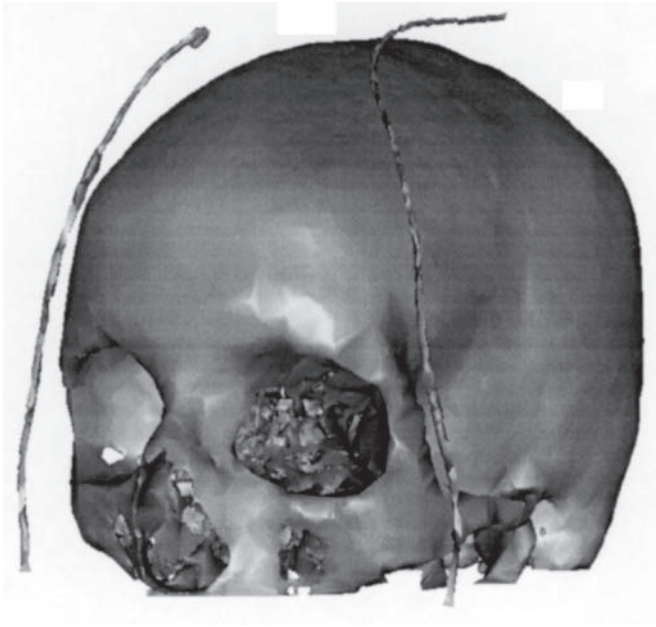

*Figure 1* Original polygonal skull constructed from the visible male data using the vtk code.

A set of planes were then constructed over half of the skull and sets of contour curves were generated at the intersection of these planes and the triangles of the model. Sections for meshing were chosen at this stage and are shown in Fig. 2 for the brain. The contour representation of the inner and outer surfaces of the skull that were thus generated are shown in Fig. 3. It was decided that the inner contours would be used to generate the finite element mesh for the brain, after first having created a uniformly deep layer which would represent the CSF. The CSF layer was created using the surface mesh of the interior surface of the skull by issuing a sweep command in the normal inwards direction by a specified distance. New curves and surfaces were then established from these resulting inner nodal positions. Solid elements were thereby created between these new surfaces and the interior surface of the skull: these elements defined the uniformly thick CSF layer.

The resulting 3-dimensional finite element model of the skull-brain complex includes; scalp, 3-layered skull (outer and inner tables, diploe), dura, CSF, pia, falx, tentorium, cerebral hemispheres, cerebellum and brain stem. Meshing was an issue that arose in previously constructed models in the literature [8, 11, 12, 18–20] but in this model much emphasis was placed on mesh quality and ease of mesh creation, without sacrificing

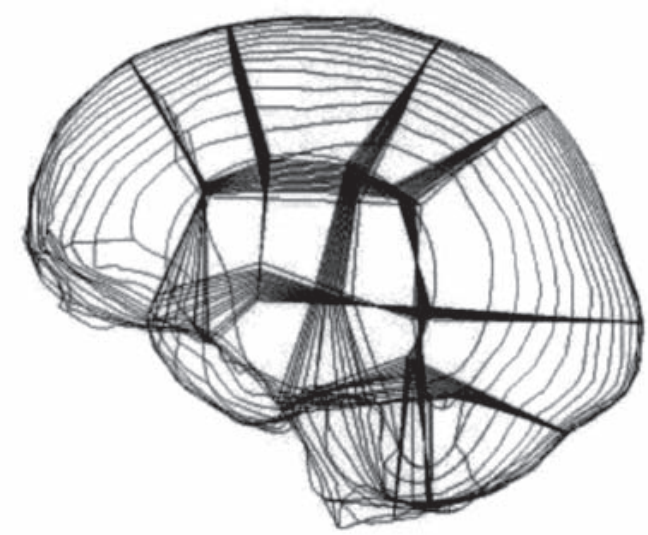

*Figure 2* Model Decomposition Sections. The sections produce well behaved elements. In the areas of high curvature (outside of cerebellum and frontal lobe), simple mesh transitioning is utilised.

anatomical accuracy. For example, the ridge of the sphenoid wing, or the cusp of the skull upon which the temporal lobe sits, does not have an element face traversing it, which would necessitate a smoothing of this ridge (for element quality), but still avoids problems which have previously arisen [18].

After initial models were constructed, it was noted that if scaling, updating and mesh parameterisation were to be investigated, the model would need to be sub-divided into sufficiently well behaved mapped meshable sections. Also from early attempts, it was noted that these sections should be sufficiently robust so as to require minimal manual manipulation of the elements of the model: this had been a problem in other published models [12]. Figure 2 shows an image of the sections that were prepared prior to meshing of the intracranial contents, and from these the finite element representation was prepared, and can be seen in Figure 5, which shows that loss in anatomical accuracy was minimised. Initially these sections were used on a contour-contour basis, i.e., a number of blocks of meshes were created and then equivalenced. This lead to a rougher appearance for the model and reduced the freedom for mesh paths to follow parametric directions, which is useful when constructing a coarse mesh. Because of this, the contours within the sections were sampled again (see Figs. 3, 4), and curves were fitted across all contour curves that were in each section, using least squares cubic curve fits or b-spline curves of various orders (these were used mainly in the area of the temporal lobe, in order to capture the change in shape from midbrain to lobe more accurately). The model associated with these curve fitted contours can be meshed quickly and used conveniently in parametric analyses.

Two different models were generated from these sections. For the first, the scalp was modelled using shell elements, cortical and trabecular bone with brick elements of varying skull thickness, the dura with membrane elements, CSF with brick elements, pia with membrane elements, falx and tentorium with shell elements and the cerebrum, cerebellum and brain stem with brick elements. The second model is similar apart from the skull being modelled using a composite shell element, the advantages of which were noted in [21], and the scalp being modelled with brick elements. A MATLAB [22] program was created to map the thickness information at the nodes from the brick elements of the skull from the first model, and apply

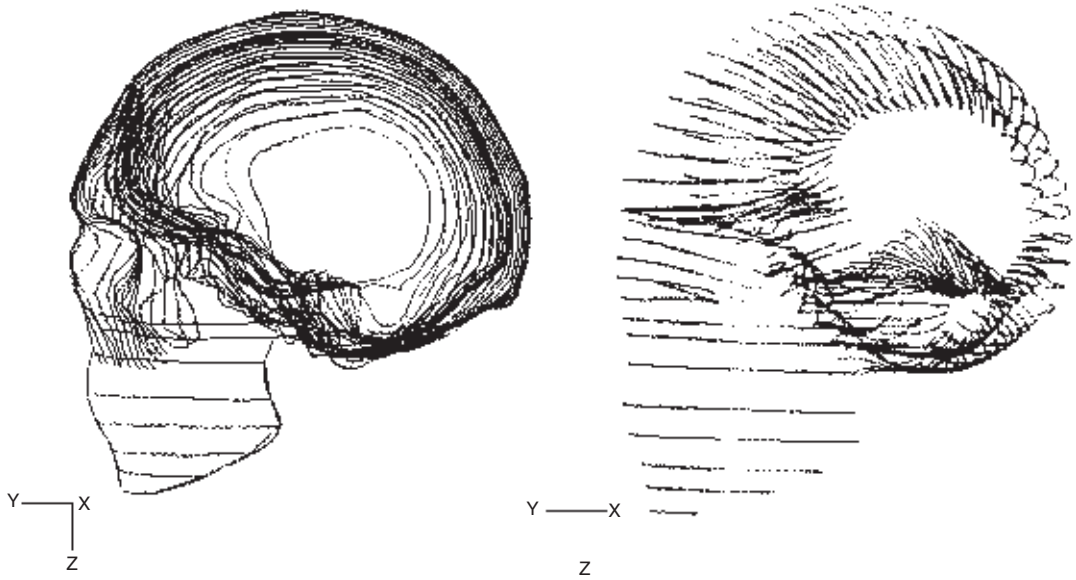


*Figure 3* Sagittal contours that were extracted from the polygonal model when planar intersections were made (horizontal planes generated contours for the side of the head; these are not shown). On the right is the overview of the splined curves generated from the contours for the entire model (excluding the side). The curve fitting method had the beneficial effect of smoothing out rough contour data.

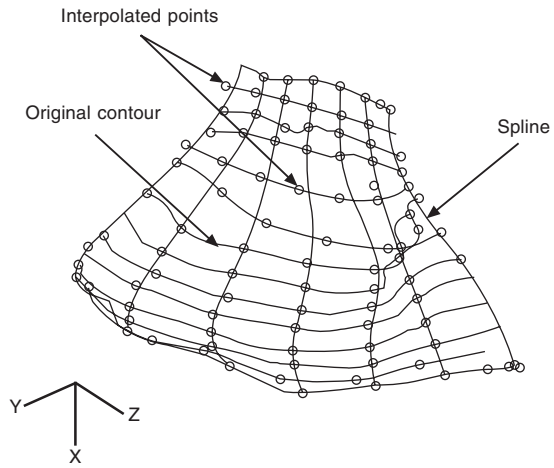


*Figure 4* Contours were extracted from cutting planes on the polygonal model. Points were then interpolated along the curves and cubic least squares curve fits or b-splined curves of various orders generated.

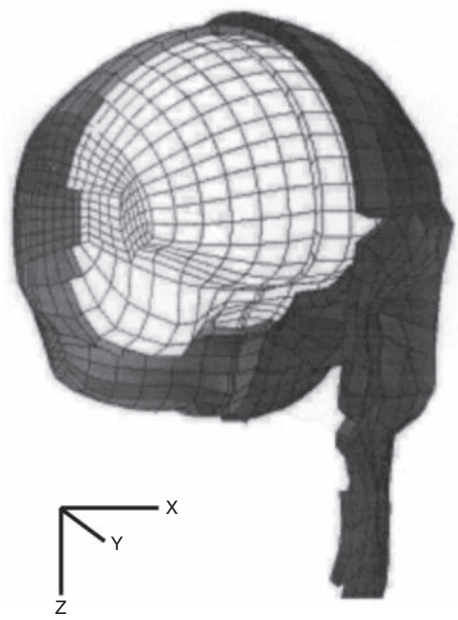


*Figure 6* Coarse mesh, 3 mm thick CSF layer. The dark elements indicate the scalp sitting on the composite skull. The grey shaded elements represent the CSF and the white elements correspond to the brain, with the cerebral trunk visible.

it as a nodal thickness definition on the shell elements of the second model. Variations of these two models were created with element densities varying from 9000 elements to 50 000 elements.

Figures 5, 6, 7 and 8 portray the two parent models that have been constructed to date. From these we have constructed:

- A fine, medium and coarse mesh with a brick element skull and a CSF depth of 1.3 mm (note: the coarsely meshed model does not include a 3 layered skull).
- A fine mesh with a brick element skull with 3 mm of CSF.
- Three shell element skull models, two with 1.3 mm CSF but with different weight and size of head and one with 3 mm, the former having the finer mesh.

## MATERIAL PROPERTIES

Identifying correct constitutive properties for neural tissue continues to be a limiting restriction in computational modelling. Earlier finite element models of the brain adopted linear elastic material constitutive laws [19, 20, 23]. In recent studies, linear viscoelastic material laws combined with large-deformation theory were used to model brain tissues [8, 24, 25], except for the work of Mendis [26], who employed nonlinear viscoelastic materials under large-deformation. It is generally believed that brain tissue is a highly damped material. Thus, a linearly viscoelastic material model combined with a large-deformation theory was chosen to model brain tissue in the present study. The behaviour of this material was characterised as viscoelastic in shear with a deviatoric stress rate dependent on the shear relaxation modulus, while the compressive behaviour of the brain was considered as

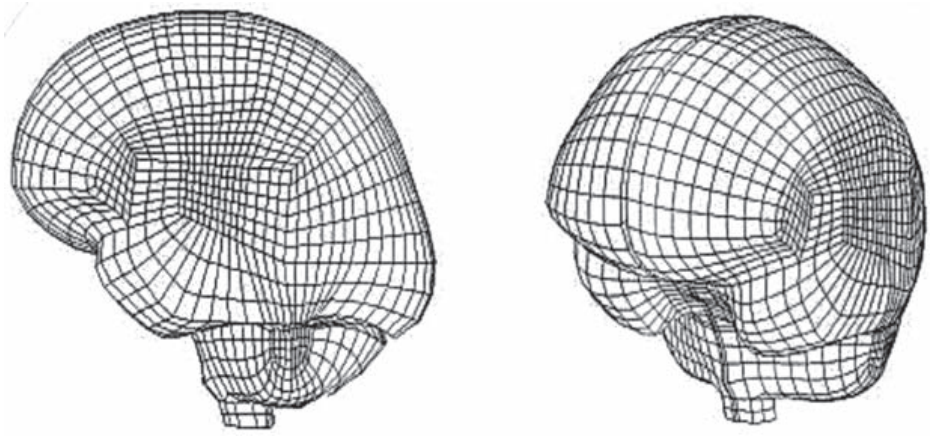

*Figure 5* Side and perspective view of the meshed brain (medium density).

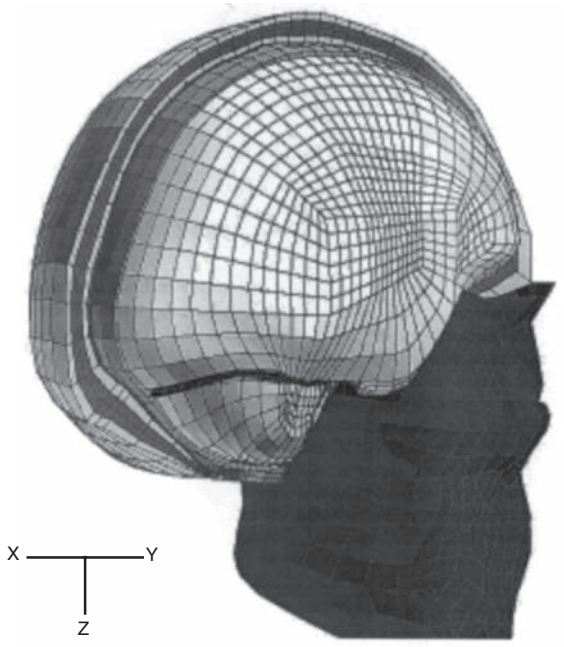


*Figure 7* Medium density mesh with 1.3 mm thick CSF layer. Dark shading represents facial bone. A section cutaway of the 3-layered skull is visible, underneath which is shown a small amount of CSF (shaded in grey). The brain elements are shown in white whilst some of the darkly shaded tentorium bone is visible.

elastic. The shear characteristics of the viscoelastic behaviour of the brain was expressed by:

$$G(t) = G_\infty + (G_0 - G_\infty)e^{-\beta t} \quad (1)$$

where $G_\infty$ is the long term shear modulus, $G_0$ is the short term shear modulus and $\beta$ is the decay factor.

The CSF layer was modelled using solid elements with a low shear modulus as has been done by others [8, 12, 21, 27, 28, 29]. Due to computational constraints, it was not feasible in the present work to model a sliding boundary condition between the interfaces of the skull/CSF/brain. The depth of the CSF layer was chosen to be either 1.3 mm or 3 mm, the former corresponding more closely to an adult and the latter to a very elderly person. The bulk modulus for the fluid was very high and as such use was made of the hybrid elements in ABAQUS [30]. Near-incompressible behaviour occurs when the bulk modulus is very much larger than the shear modulus (usually where the Poisson's ratio is greater than 0.48) and exhibits behaviour approaching the incompressible limit: a very small change in displacement produces extremely large changes in pressure. Therefore, a purely displacement–based solution is too sensitive to be useful numerically. This singular behaviour is removed from the calculations in ABAQUS by treating the pressure stress as an independently interpolated basic solution variable, coupled to the displacement solution through the constitutive theory

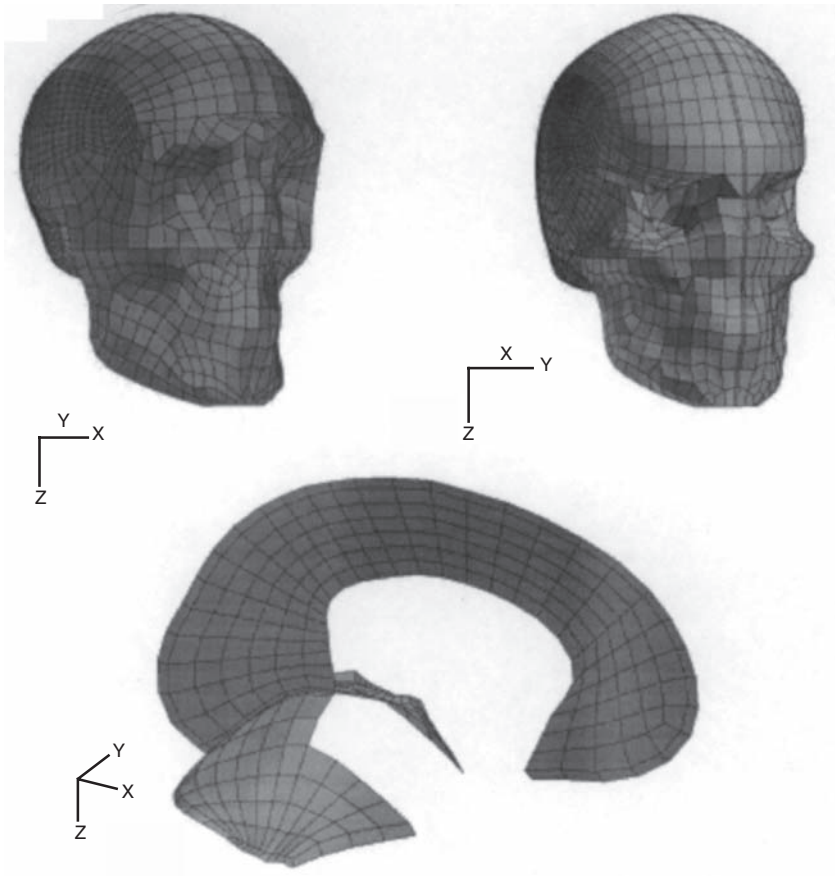


*Figure 8* Perspective images of the two head models with the intracranial membranes.

and the compatibility condition. This independent interpolation of pressure stress is the basis of the hybrid element.

The material properties for the remaining parts of the model, i.e., the cortical and trabecular bone, scalp and intracranial membranes were taken from the literature [8, 10, 12, 31]. Table 1 summarises the mechanical properties that were used in the subsequent analyses. The weight of the model when scaled to the dimensions of the cadaver skull of experiment 37 of Nahum [3] was 4.017 kg whilst the brain weighed 1.422 kg. The inertial properties are $I_{YY}$ = 1795 kg.mm$^2$, $I_{ZZ}$ = 1572 kg.mm$^2$ and $I_{XX}$ = 1315 kg.mm$^2$, similar to those of Kleiven [10].

*Table 1* **Table of material properties**

| Material | Young's modulus (MPa) | Poisson's ratio | Density (kg/m$^3$) |
|---|---|---|---|
| Scalp | 16.7 | 0.42 | 1000 |
| Cortical Bone | 15 000 | 0.22 | 2000 |
| Trabecular Bone | 1000 | 0.24 | 1300 |
| Dura | 31.5 | 0.45 | 1130 |
| Pia | 11.5 | 0.45 | 1130 |
| Falx and Tentorium | 31.5 | 0.45 | 1130 |
| Brain | Hyper Elastic | 0.499981 | 1040 |
| Facial Bone | 5000 | 0.23 | 2100 |

## VALIDATION OF MODEL

The model was validated by simulating the cadaveric head impact experiments of Nahum et al. [3] and by directly comparing the predicted pressure-time histories against those obtained experimentally. The analysis was undertaken using ABAQUS 5.8 [30].

The model was oriented in the same manner as Nahum's original experiment. The head was rotated forward at 45° to the frankfort plane. A frontal impulse was applied in the sagittal plane in an anterior to posterior direction. The load form was approximately a semi-sinusoidal pulse of peak magnatude 7000N and duration 6 ms. Since the neck restraint is unlikely to affect the head response in a short duration (<6 ms) impact [8], a free boundary condition was assumed in the analysis. Figure 9 shows the correlation of the simulated and experimental pressure time histories for the impact. Figure 10 shows the pressure response at the peak of the impact force and Figure 11 shows the corresponding Von Mises stress at that same instant.

The model used for validation was the medium meshed

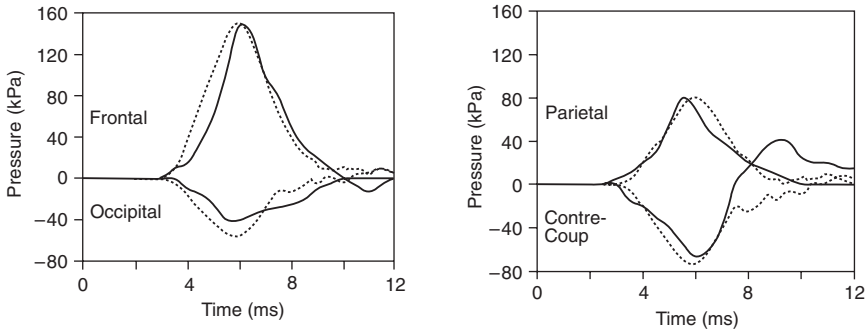


*Figure 9* Comparison between the experimental intra-cranial pressures of Nahum (solid lines), and those predicted by simulation (dashed lines) using the model warped to Nahum's dimensions.

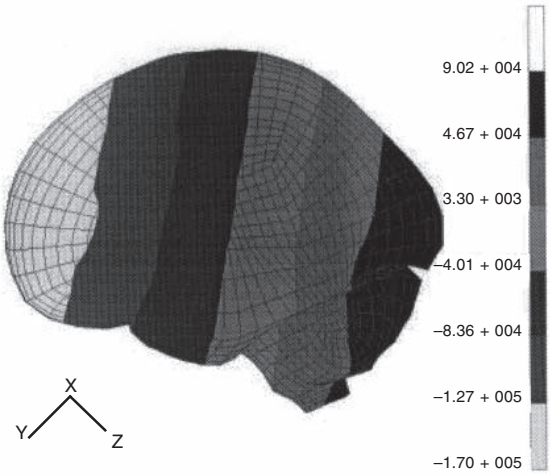


*Figure 10* Hydrostatic pressure response of the brain (in Pa) of the model at the peak of the impact pulse.

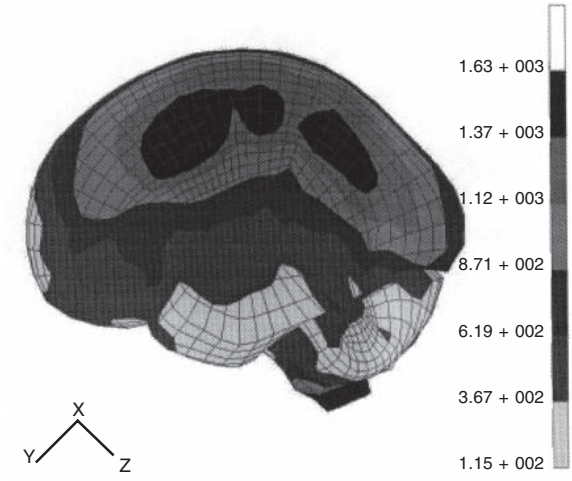


*Figure 11* Von Mises (in Pa) response for the brain at the peak of the impact pulse.

model with a thin CSF depth. It was warped to the dimensions of the cadaver head of experiment 37 of Nahum. It used the material properties of Mendis [26] as were also used by Kleiven [10]. A hyperelastic material was used for the brain to maintain these properties, in conjunction with a viscoelastic material property as is possible in ABAQUS [30], giving the material a decay factor of $\beta = 145\ s^{-1}$. The hyperelastic law was given by:

$$C_{10}(t) = 0.9C_{01}(t) = 620.5 + 1930e^{-t/0.008} + 1103e^{-t/0.15}(\text{Pa}) \quad (2)$$

where $C_{10}$ and $C_{01}$ are temperature-dependent material parameters, and time $t$ is in seconds.

The experimental results obtained by Nahum are not full-field data, unlike those of the present FE simulations. Rather, they are discrete point-wise results that were obtained from transducers located at particular regions of the head. In order to compare the present simulations with the experimental results, four specific locations were selected from the FE model, namely (i) the coup site, adjacent to the impact site, (ii) the parietal site, (iii) the occipital site and (iv) the contrecoup site, opposite the impact site.

The correlation is good and as such the model can be considered to be validated. The maximum values achieved, the shape of the response and the duration of the effect all match quite well with that of the experimental results.

## PARAMETRIC ANALYSES

Using the same impulse load condition of the previous section, numerous simulations were completed in an attempt to identify the effects of changing material properties of the brain and CSF. Table 2 identifies the values of the parametrically varied elastic properties of the neural tissue and cerebrospinal fluid: the bulk and shear moduli. All other properties remained as specified in Table 1. Simulations were also carried out using different head weights, mesh densities, CSF depths and model dimensions. (adjusted Willinger [21] properties, the bulk modulus of the fluid was increased by one order of magnitude to become $2 \times 10^6$ Pa). For example, it was of interest to consider the possible response of the model when:

A it was warped, i.e. scaled by different amounts in the X, Y and Z dimensions, to those dimensions of Nahum and
B when it was scaled *globally* to the size of Nahum using a global characteristic length proposed by Mertz [32]:

$$\lambda_X = \lambda_Y = \lambda_Z = \frac{(C + W + L)_S}{(C + W + L)_H} \quad (3)$$

where $\lambda_X$, $\lambda_Y$, $\lambda_Z$ are the length scale factors, $C$ = head circumference, $W$ = head width, $L$ = head length and subscripts S and H refer to the subject and the base model respectively (in Mertz's case, it was H for the Hybrid III dummy). The motivation for this comparative analysis is that when the 'warping' method (method A), is used there is no guarantee that the inner skull dimensions have been correctly scaled although the outer dimensions of the skull may equal those of Nahum. With the method of Mertz (method B), while the dimensions of the original visible male's brain may be changed, its overall shape will not deviate.

### Influence of constitutive properties

A series of High/Low tests was carried out on the coarse model to investigate the influence of the shear modulus and bulk modulus of both the brain and the CSF, while all other properties were kept the same (the effects of the decay rate and the long term shear modulus were not modelled here). These tests consisted of taking a low and a high value for the properties in question, and carrying out a series of tests which would include all possible permutations. Therefore, when considering the state of the model in a high or a low state (a 1 or 0 state respectively), across 4 different influencing factors, $2^4$ tests must be run. The results for the High-Low tests are given in Table 2. The values of hydrostatic stress reported in the table are those at the moment of maximum impact pulse. Superscripts 'd' and 'e' indicate that the actual maximum stresses occurred at a time that was either delayed or earlier than the moment of maximum impact pulse. To investigate the effect of the brain's shear modulus, for example, tests 0-0-0-0 and 1-0-0-0 can be compared, as can tests 0-1-1-1 and 1-1-1-1, and tests 0-1-0-0 and 1-1-0-0, etc. A sample set of graphs of the effects is shown in Figures 12 (a)–(f), in which hydrostatic stress rather than pressure is plotted on the lefthand axis. The solid curves in the graphs of Figures 12 (a)–(f) refer to the hydrostatic stresses (negative pressures) in the frontal, occipital, parietal and contrecoup regions of the brain, similar to the regions considered in the previous section. The dotted curves in Figures 12 (a)–(f) (referring to the righthand axis) indicate the variation of Von-Mises stress for the corpus callosum.

The shear modulus of the brain was seen to have a very large effect on the intracranial pressure, in both the frontal and contrecoup regions, and on the Von-Mises response. Specifically, an increase in the shear modulus would decrease the frontal pressure, increase the contrecoup pressure, and increase the Von-Mises stress at the corpus callosum.

The bulk modulus of the brain seemed to have little effect on either the pressures or the Von-Mises response, although it is likely that if a larger decrease in bulk modulus value was chosen, that the effect would be more apparent (more specifically, if the 'low' value had been lower, as the material is already approaching incompressibility at these values).

Looking at the effect of the bulk modulus of the CSF, it is evident that while it can reduce the pressure sustained by the frontal lobe, when the value is as low as it is in this test, it also delays the time at which maximum stress is achieved. Such a phase shift was not apparent in the

*Table 2* **High/Low results using the coarsely meshed model with the original visible male's dimensions. Also included is a comparison of the properties using Ruan [8], Zhou [12] and Willinger [21]. Superscripts 'd' and 'e' refer to a simulation in which the actual peak value occurred after or before (i.e., delayed or early, respectively) the peak of the impact pulse**

| Case | Shear modulus (kPa) | Bulk modulus (MPa) | Frontal pressure (kPa) | Contre-coup pressure (kPa) | Von-Mises (Pa) |
|---|---|---|---|---|---|
| 0-0 | Brain = 20 | Brain = 200 | $223^d$ | $-37.5^e$ | 23 800 |
| 0-0 | CSF = 0.5 | CSF = 0.25 | | | |
| 0-0 | Brain = 20 | Brain = 200 | $221^d$ | $-32.5^e$ | $4528^d$ |
| 0-1 | CSF = 0.5 | CSF = $2.5 \times 10^3$ | | | |
| 0-0 | Brain = 20 | Brain = 200 | $156^d$ | $-91^d$ | $11\,320^d$ |
| 1-0 | CSF = 50 | CSF = 0.25 | | | |
| 0-1 | Brain = 20 | Brain = $20 \times 10^3$ | 195 | $-110.5^d$ | $4245^d$ |
| 0-0 | CSF = 0.5 | CSF = 0.25 | | | |
| 1-0 | Brain = 500 | Brain = 200 | $160^d$ | $-80^d$ | $2.5 \times 10^5$ |
| 0-0 | CSF = 0.5 | CSF = 0.25 | | | |
| 0-0 | Brain = 20 | Brain = 200 | 210 | $-30^e$ | $2500^d$ |
| 1-1 | CSF = 50 | CSF = $2.5 \times 10^3$ | | | |
| 0-1 | Brain = 20 | Brain = $20 \times 10^3$ | $150^d$ | $-90^d$ | $11\,500^d$ |
| 1-0 | CSF = 50 | CSF = 0.25 | | | |
| 1-1 | Brain = 500 | Brain = $20 \times 10^3$ | $160^d$ | $-80^d$ | $2.2 \times 10^5$ |
| 0-0 | CSF = 0.5 | CSF = 0.25 | | | |
| 0-1 | Brain = 20 | Brain = $20 \times 10^3$ | 230 | $-30^e$ | 4000 |
| 0-1 | CSF = 0.5 | CSF = $2.5 \times 10^3$ | | | |
| 1-0 | Brain = 500 | Brain = 200 | $100^d$ | –55 | $1.35 \times 10^5$ |
| 1-0 | CSF = 50 | CSF = 0.25 | | | |
| 1-0 | Brain = 500 | Brain = 200 | 165 | –91 | $42\,000^d$ |
| 0-1 | CSF = 0.5 | CSF = $2.5 \times 10^3$ | | | |
| 0-1 | Brain = 20 | Brain = $20 \times 10^3$ | 235 | $-30^e$ | $2338^d$ |
| 1-1 | CSF = 50 | CSF = $2.5 \times 10^3$ | | | |
| 1-1 | Brain = 500 | Brain = $20 \times 10^3$ | 108 | –54 | $135\,000^d$ |
| 1-0 | CSF = 50 | CSF = 0.25 | | | |
| 1-0 | Brain = 500 | Brain = 200 | 162.5 | –97.5 | $25\,515^d$ |
| 1-1 | CSF = 50 | CSF = $2.5 \times 10^3$ | | | |
| 1-1 | Brain = 500 | Brain = $20 \times 10^3$ | 200 | $-58.5^e$ | $40\,500^d$ |
| 0-1 | CSF = 0.5 | CSF = $2.5 \times 10^3$ | | | |
| 1-1 | Brain = 500 | Brain = $20 \times 10^3$ | 185 | $-60^e$ | $22\,500^d$ |
| 1-1 | CSF = 50 | CSF = $2.5 \times 10^3$ | | | |
| Ruan [8, 1994] | Brain = 186 CSF = 50 | Brain = 93 CSF = 1.65 | 145 | -105 | 26 300 |
| Zhou [12, 1995] | Brain = 268 CSF = 50 | Brain = $3.49 \times 10^2$ CSF = 21.9 | 145 | –70 | 13 800 |
| Willinger [21, 1999] | Brain = 49 CSF = 4 | Brain = $1.11 \times 10^3$ CSF = 0.2 | $160^d$ | $-80^d$ | 41 500 |

experiments of Nahum. When it is set low, it can also be seen that this causes numerical oscillations after the impulse has been applied.

The shear modulus of the fluid seemed to have little effect, apart from visually. When a higher value was used, the pressure contours were very uniform at the peak of the impulse, whereas when the value was set low, the edges of the contours were less defined.

Also of interest was the different Von-Mises stresses produced in the model. As can be seen in the set of sample graphs (Figures 12(a)–(f)), the shape of the curves varied quite significantly. When the shear modulus of the brain was set low, the Von-Mises stress continues to rise after the peak of the impulse. When it is set high, it seems to have a peak itself and then falls off (it should be noted that values denoted with a 'd' in the table refer strictly to when the peak occurred after the peak of the impulse and not that it continued to rise).

The models were also run using the material properties of Ruan [8], Zhou [12], and Willinger [21], and the results are given both in Table 2 and Figure 13. It can be seen that, for this particular model, use of the properties of Zhou provided the best correlation with experiment. It should be noted, however, that the density of the homogenous skull used in Zhou's test and also here, was heavier than that used for our test with Ruan's and

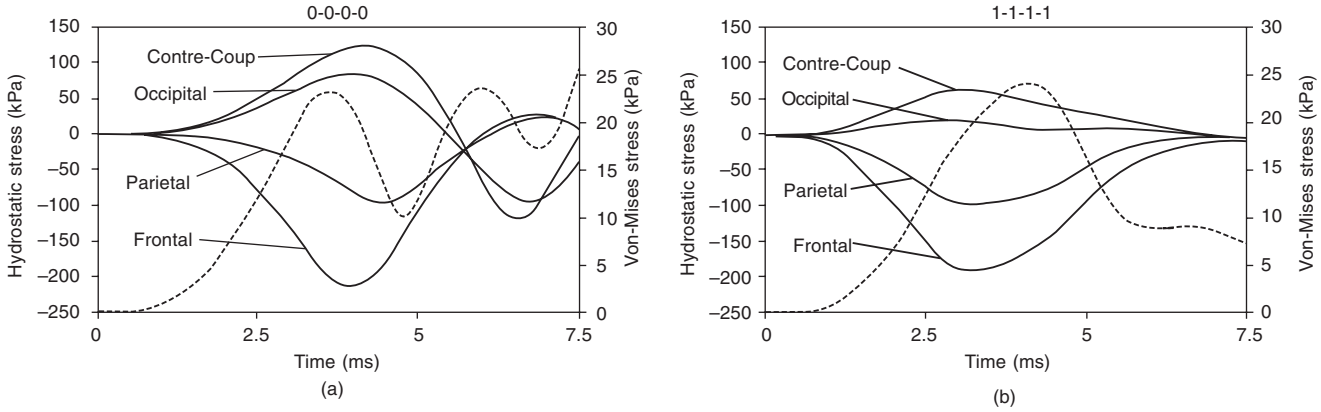


*Figure 12* Comparison when all properties were set low (a), with when all properties were set high (b). The solid lines are the hydrostatic stress results and refer to the lefthand axis, while the dotted lines are the Von-Mises results and refer to the righthand axis.

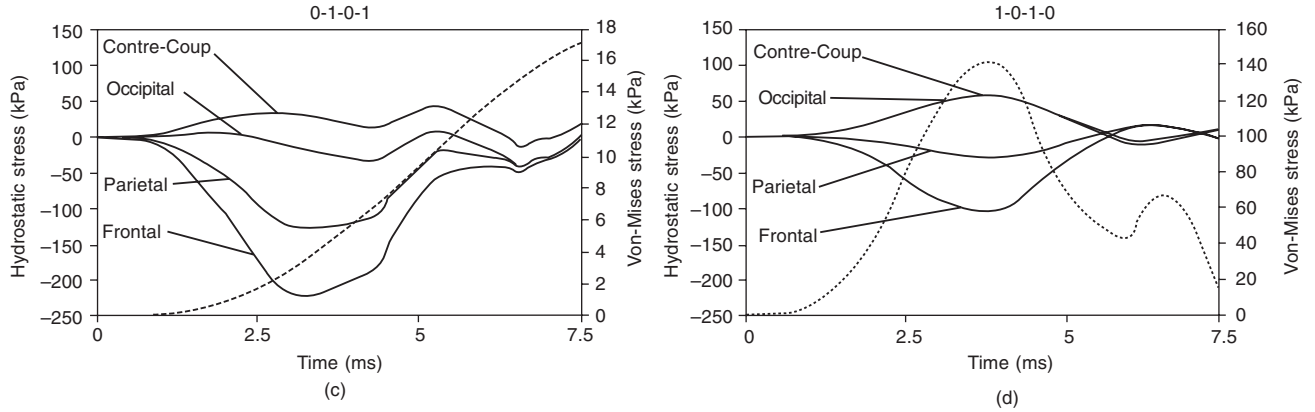


*Figure 12* Comparison when both Brain and CSF have low shear moduli and high bulk moduli (c), with the reverse case (d). The solid lines are the hydrostatic stress results and refer to the lefthand axis, while the dotted lines are the Von-Mises results and refer to the righthand axis (note: scales on righthand axes are not equal).

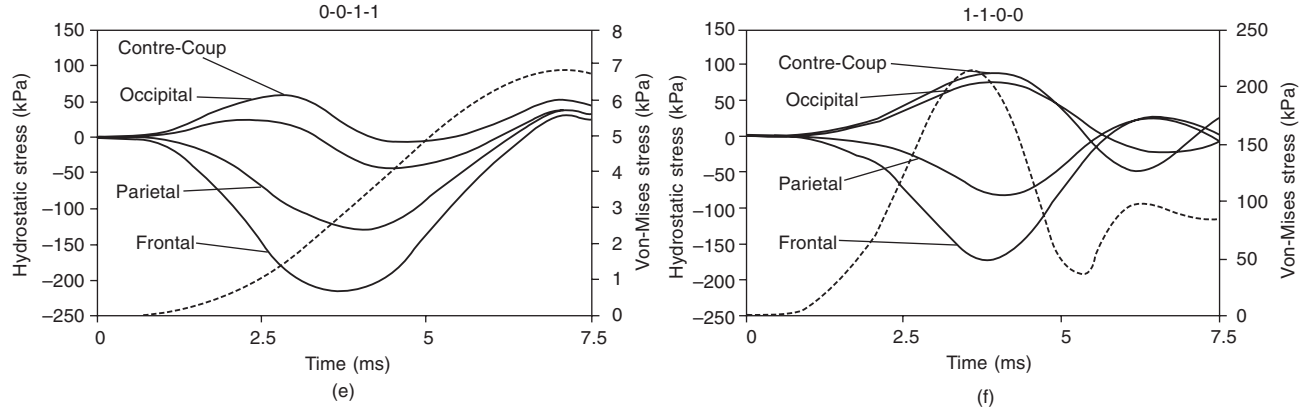


*Figure 12* Comparison when all brain properties were set low and CSF properties set high (e), with the reverse case (f). The solid lines are the hydrostatic stress results and refer to the lefthand axis, while the dotted lines are the Von-Mises results and refer to the righthand axis (note: scales on righthand axes are not equal).

Willinger's properties (Zhou's homogeneous skull had a density of 2100 kg/m$^3$, making the model weigh 4.08 kg and not 3.308 kg).

### Tests across models

The effect of using different finite element models was addressed by using the same input conditions and material properties for the brain and CSF. The adjusted value of CSF from that of Willinger was chosen as this increase led to less oscillation after the impulse, and removed the delayed peaks which had been present with the lower value. As in the tests of the previous section, all properties were

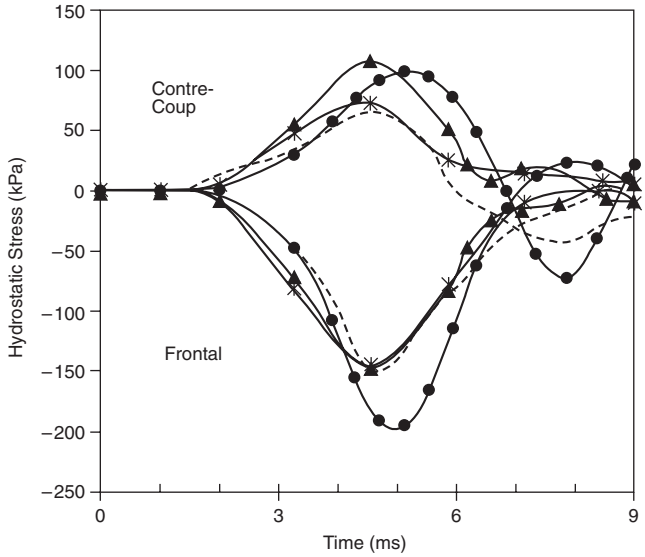


*Figure 13* Graph comparing results when the material properties of Ruan [8] (solid triangles), Zhou [12] (crosses) and Willinger [21] (solid circles) were used with this model, against the experimental results of Nahum [3] (dashed line).

treated as purely elastic and isotropic. The results are shown in Tables [3–6] and a sample image of two of the models at the peak of the impact pulse is shown in Figure 14.

Table 3 compares the different results predicted by models of different physical size. A heavier model predicts lower intracranial pressure. This agrees with Nahum who reported that higher accelerations produce higher intracranial pressures. Using Newton's basic relationship, when the same impulse is applied to a heavier head, the acceleration, and hence the pressure, is reduced.

A deeper fluid depth seems to reduce the frontal pressure, but also slightly increases the contre-coup pressure, as seen in Table 4. These few results indicate

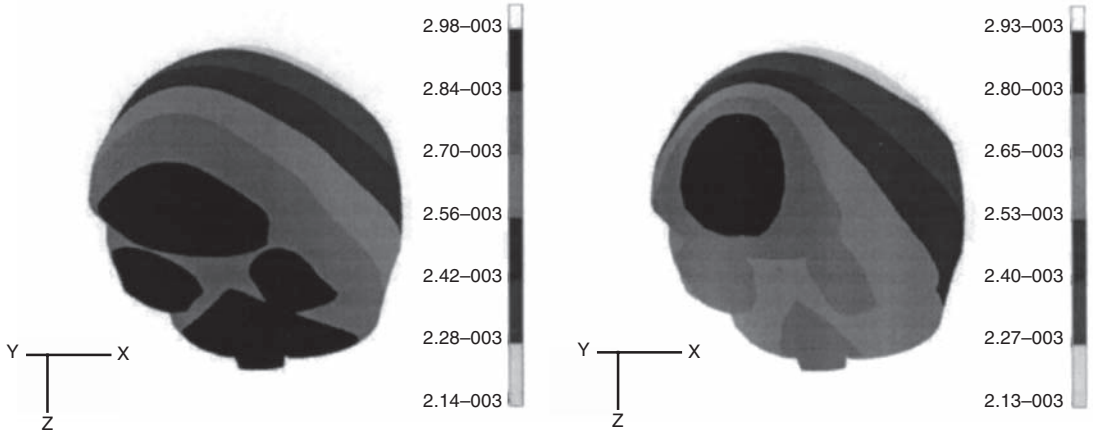


*Figure 14* Displacement plot comparison of two of the models. On the left is the brick-brick skull model, Nahum Warped, and on the right is the Shell-Brick model. The plot is of the dura, which has coupled nodes with the inner surface of the skull.

*Table 3* **Comparison across models of different sizes of models (superscripts are as before)**

| Model | CSF depth | Weight (kg) | Mesh density | Frontal pressure (kPa) | Contre-coup pressure (kPa) | Von-Mises (Pa) |
|---|---|---|---|---|---|---|
| Visible Male | Thin | 3.308 | Coarse | 170 | –105 | 11 000[d] |
| Nahum Warped | Thin | 4.02 | Medium | 150 | –100 | 3800 |
| 50th-percentile [33] | Thin | 4.14 | Coarse | 150 | –85[e] | 6900 |
| Scaled to weight (Shell skull) | Thin | 4.7 | Medium | 145 | –85[e] | 5400[e] |

that the Von-Mises stress is greatly affected by the depth of CSF. Comparing the scaled to weight models, for example (simple scaling to match the weight of the model of Willinger [21]), the model with a 3 mm depth of CSF depth predicted a value of 10000Pa, almost double that of the model with less CSF.

Three types of skull formulation were investigated and these are summarised in Table 5. These models were (i) a 4 brick element deep model, where the middle two layers of brick elements were assigned to be trabecular bone, (ii) a composite shell element model, which assigned 2 mm for cortical bone and 3 mm for trabecular bone (similar to [21]), and (iii) a shell-brick model where the cortical bone was assigned to be a shell element (included with either the scalp or the dural definitions), and the trabecular bone was assigned to be brick elements (as done by [10, 34]). Use of type (iii) skull shows a reduction in intracranial pressure, which we believe is due to the increased presence of 'spongy' bone (and not due to any increase of thickness of the skull, as the shell thickness chosen for the cortical bone was small). It also lead to a small increase in contre-coup pressure and Von-Mises stress and this pattern was also observed in other tests which are not reported in this paper. Use of the type (ii) model (composite shell element) reports higher values of pressure when compared with similar intracranial geometry, with an associated drop in contre-coup pressure and similar Von-Mises stress results. The difference in displacement shape patterns for the type (i) and type (iii) models can be seen in Figure 14. The 'shell-brick' skull model shows a higher concentration of displacement at the impact site, where the 'all brick' model shows a more banded response.

Table 6 presents the different predictions when the model was scaled using warping or the characteristic length scaling of Mertz [32]. The latter method showed a decreased frontal pressure at a similar measuring point to the warped model. While further testing would be required for a full investigation, it is believed that the different shapes of the frontal lobes caused this difference. Namely, the Mertz scaled model has a larger major axis and smaller minor

*Table 4* **Comparison across models of different CSF depths**

| Model | CSF depth | Weight (kg) | Mesh density | Frontal pressure (kPa) | Contre-coup pressure (kPa) | Von-Mises (Pa) |
|---|---|---|---|---|---|---|
| Visible male (Shell skull) | Thin | 3.41* | Medium | 190 | –90[e] | 6750 |
| Visible male (Shell skull) | Deep | 3.39 | Coarse | 165 | –120 | 11 000 |
| Visible male | Thin | 3.785 | Fine | 154 | –93 | 6250[d] |
| Visible male | Deep | 3.595 | Fine | 145 | –125 | 13 000[d] |
| Scaled to weight (Shell skull) | Thin | 4.7 | Medium | 145 | –85[e] | 5400[e] |
| Scaled to weight (Shell skull) | Deep | 4.7 | Coarse | 135 | –95 | 10 000 |

*Inclusion of scalp on face contributes to some difference in weight.

*Table 5* **Comparison across models of different skull types (skull element formulation is mentioned in brackets)**

| Model (Skull formulation) | CSF depth | Weight (kg) | Mesh density | Frontal pressure (kPa) | Contre-coup Pressure (kPa) | Von-Mises (Pa) |
|---|---|---|---|---|---|---|
| Visible male (Brick) | Thin | 3.308 | Coarse | 170 | –105 | 11 000[d] |
| Visible male (Shell skull) | Thin | 3.41 | Medium | 190 | –90[e] | 6750 |
| Nahum warped (Brick) | Thin | 4.02 | Medium | 150 | –100 | 3800 |
| Scaled to weight (Shell skull) | Thin | 4.7 | Medium | 145 | –85[e] | 5400[e] |
| Nahum warped (Shell-brick) | Thin | 3.819 | Medium† | 135 | –105 | 4860 |

†Shell elements for the cortical bone

*Table 6* **Intracranial shape variations**

| Model | CSF depth | Weight (kg) | Mesh density | Frontal pressure (kPa) | Contre-coup pressure (kPa) | Von-Mises (Pa) |
|---|---|---|---|---|---|---|
| Nahum warped | Thin | 4.02 | Medium | 150 | –100 | 3800 |
| Mertz global scale Nahum | Thin | 4.2 | Medium | 135 | –100 | 5400[d] |
| Scaled to weight (Shell skull) | Thin | 4.7 | Medium | 145 | –85[e] | 5400[e] |
| Scaled to weight (Shell skull) | Thin | ~4.7 | Medium[‡] | 130 | –70 | 4580[e] |

[‡]Varying thickness shell element skull

axis than the model warped to the dimensions of Nahum's experiment 37, in terms of the prolate ellipsoid. Also a test was run with the thickness information mapped from the brick element model to be given in the definition for the shell element model. As can be seen from the results, the pressures are reduced and there is a smaller displacement at the impact site. This would be due to the increased skull thickness at that site absorbing more of the load. Overall the skull is heavier with the varying thickness and, as was said in earlier in this section, this would lead to a drop in the pressure.

## CONCLUSIONS

A 3-dimensional model of the skull-brain complex has been constructed. The method by which it was built has been reported and it is suggested that this procedure could be used by others who would also wish to develop separate skull-brain models.

The model was validated against the cadaver impacts performed by Nahum [3]. The model was also scaled and warped so as to represent the same size head as that used in Nahum's experiment. A parametric study was performed to investigate the effect of different mesh densities on the models, the use of a composite shell element skull, and the influence of material properties.

By considering the values from Table 2 it was found that the short term shear modulus of the neural tissue had the biggest effect on intracranial frontal pressure, and on the model's Von-Mises response. The bulk modulus of the fluid had a significant effect on the contre-coup pressure when the CSF was modelled using a coupled node definition. The differences of this particular model's response when using the material properties of Ruan [8], Zhou [12], and Willinger [21] was correlated: those properties of Zhou gave best agreement with the cadavaric experiments of Nahum.

A comparison between different mesh densities showed that a coarsely meshed model is adequate for investigating the pressure response of the model, while a finer mesh is more appropriate for detailed investigations. The effect of modeling the skull using composite shell elements was also compared to the use of brick elements. Although this would improve the speed of calculations in itself, modeling the scalp as a brick element lead to a large increase in the number of increments required to obtain a convergent solution (using the tight tolerances required for implicit solvers). The scalp can be included into the composite shell element definition, but without the inclusion of the thickness varying at the nodes, and with the loss of the failure prediction capabilities.

By simulating identical impact scenarios with a range of different finite element models it has been possible to investigate the influence of model geometries. We can conclude that careful modelling of the CSF (depth/volume) and skull thickness is necessary if the correct intracranial pressure distribution is to be predicted. Furthermore, if the physical dimensions of the particular human head being modelled are known, the finite element model should be scaled to these dimensions.

Subsequent research will further refine the present 3D model, by including bridging veins and by distinguishing between white, grey and ventricular matter. It is proposed to use this model for an accident reconstruction study of patients who have suffered simple falls [35, 36]. This will be discussed separately elsewhere.

## References


1. Meaney, D F, Thibault, L E and Gennarelli, T A. Rotational brain injury tolerance criteria as a function of vehicle crash parameters. In *Proc. of the 1994 International IRCOBI Conf. on the Biomechanics of Impacts, pages* 51–62, 1994.
2. Trosseille, X, Chamourd, F and Tarriere, C. Reconsideration of the HIC, taking into account the skull bone condition factor (SBCF) – limit of head tolerance in side impacts. In *Proc. of the 32nd Stapp Car Crash Conf*, SAE paper no. 881710, 1988.
3. Nahum, A M, Smith, R W and Ward, C C. Intracranial pressure dynamics during head impact. In *Proc. of the 21st Stapp Car Crash Conf*, SAE paper no. 770922, 1977.
4. Misra, J C and Chakravarty, S. A study on rotational brain injury. ASME J. *Biomech. Eng.*, 17:459–466, 1983.
5. Goldsmith, W. *Biomechanics of Head Injury, Biomechanics, Its Foundations and Objectives*. Prentice-Hall, 1972.

6. Gurdjian, E S. Recent advances in the study of the mechanism of impact injury of the head – a summary. *Clin. Neurosurg*, 18: 1–42, 1972.
7. Holbourn, A H S. Mechanics of head injuries. *Lancet*, 2: 438–441, 1943.
8. Ruan, J S. *Impact Biomechanics of Head Injury by Mathematical Modeling*. PhD thesis, Wayne State University, 1994.
9. Edberg, S, Rieker, J and Angrist, A. Study of impact pressure and acceleration in plastic skull models. *Labs. Invest*., 12: 1305–1311, 1963.
10. Kleiven, S, and Holst, H von. Consequences of size following trauma to the human head. *J. Biomechanics*, 35:135–160, 2002.
11. Willinger, R, Kopp, C M, and Cesari, D. New concept of contrecoup lesions: Modal analysis of a finite element head model. In *Proc. of the 1992 International IRCOBI Conf. on the Biomechanics of Impacts*, pages 283–298.
12. Zhou, C, Khalil, T B and King, A. Viscoelastic response of the human brain to sagittal and lateral rotational acceleration by finite element analysis. In *Proc. of the 1996 International IRCOBI Conf. on the Biomechanics of Impacts*, pages 35–48, 1996.
13. Lee, E S. *A Large-Strain, Transient-dynamic Analysis of Head Injury Problems by the Finite Element Method*. PhD thesis, Georgia Institute of Technology, 1990.
14. Sauren, A A H J and Claessens, M H A. Finite element modelling of head impact: The second decade. In *Proc. of the 1993 International IRCOBI Conf. on the Biomechanics of Impacts*, pages 241–251, 1993.
15. National Institutes of Health (NIH) U.S. National Library of Medicine. Department of health and human services. Visible Human Database www.nlm.nih.gov/research/visible/visible human.html.
16. Lorenson, B. Vtk open source software. http://public.kitware.com/VTK/.
17. Patran r2a. *MSC/Patran User's Manual*. MSC, 2002.
18. Claessens, M, Sauren, A A H J and Wismans, J S H M. Modeling of the human head under impact conditions: A parametric study. In *41st Stapp Car Crash Conf, SAE Paper No. 973338, Society of Automotive Engineers*, pages 315–328, 1997.
19. Shugar, T A and Katona, M G. Development of a finite element head injury model. *ASCE J. Eng. Mech. Div.*, EM3(E101/173):223–239, 1975.
20. Ward, C and Thompson, R. The development of a detailed finite element brain model. In *Proc. 19th Stapp Car Crash Conference . SAE Paper No.751163*, 1975.
21. Kang, H, Willinger, R and Diaw, B M. Validation of a 3d anatomic human head model and replication of head impact in motorcycle accident by finite element modeling. In *Proceedings of the 41st Stapp Car Crash Conference*., pages 329–338, 1997.
22. MATLAB 5.6. *MATLAB User's Manual*. MATHWORKS, 2000.
23. Hosey, R R and Liu, Y K. Finite element in biomechanics. In Johnson, B R, Gallagher, T C, Simon, R H and Gross, J F. editors, *A Homeomorphic Finite Element Model of the Human Head and Neck*, pages 379–401. Wiley, 1982.
24. DiMasi, F, Marcus, J H and Eppinger, R H. 3-d anatomic brain for relating cortical strains to automobile crash loading. In *Proc. 13th Int . Tech. Conference. on Experimental Safety Vehicles*, Paper No. 91–S8–O–11, 1991.
25. Turquier, F, Kang, H S, Trosseille, X, Willinger, R, Lavaste, F, Tarriere, C and Domont, A. Validation study of a 3d finite element head model against experimental data. *Proc. of the 40th Stapp Car Crash Conf., SAE paper no. 962431*, 1996.
26. Mendis, K K, Stalnaker, R L and Advani, S H. A constitutive relationship for large deformation finite element modeling of brain tissue. *Journal of Biomechanical Engineering*, 117(4): 279–285, 1995.
27. Hu, Hao, Nayfeh, A H and Rosenberg, W S. Modeling of human brain movability during impact. In *5th International LS_DYNA Users Conference*, 1998.
28. Gilchrist, M D and O'Donoghue, D. Simulation of the development of frontal head impact injury. *Computational Mechanics*, 26(3):229–235, 2000.
29. Gilchrist, M D, O'Donoghue, D, and Horgan, T. A two-dimensional analysis of the biomechanics of frontal and occipital head impact injuries. *Int. J. Crashworthiness*, 6(2):253–262, 2001.
30. ABAQUS 5.8. *ABAQUS/Standard User's Manual*. HKS, 2000.
31. Willinger, R, Taleb, L and Kopp, C M. Modal and temporal analysis of head mathematical models. *J. Neurotrauma*, Vol. 12:743–754, 1995.
32. Mertz, H J. Size, weight and biomechanical impact response requirements for adult size small female and large male dummies. In *SP-782-Automotive Frontal Impacts, SAE Paper No. 890756, Society of Automotive Engineers*, pages 133–144, 1989.
33. Pheasant, S. *Bodyspace, Anthropometry, Ergonomics and the design of work*. Taylor & Francis, 2 edition, 1996.
34. Zhou, C, Khalil, T B and King, A I. A new model comparing impact responses of the homogeneous and inhomogeneous human brain. *In 39th Stapp Car Crash Conf., Society of Automotive Engineers*, pages 121137, 1995.
35. O'Riordain, K, Thomas, P M, Phillips, J P and Gilchrist, M D. Reconstruction of real world head injury accidents resulting from falls using multibody dynamics. In *International Conference on Computational Engineering & Science*, paper 81, 2001.
36. O'Riordain, K, Thomas, P M, Phillips, J P and Gilchrist, M D. Reconstruction of real world head injury accidents resulting from falls using multibody dynamics. *In Press, Clinical Biomechanics*.


 